Journal Homepage: https://dergipark.org.tr/tr/pub/isibted

Isı Bilimi ve Tekniği Dergisi

Archive: https://tibtd.org.tr/dergi

Optimizing Thermal Efficiency in Diesel Engines: Predicting Performance with Ternary Blends, Variable Injection Pressures and EGR Using LSTM Machine Learning

Karthikeyan SUBRAMANIAN [1], A. Paramasivam SATHIYAGNANAM [2], Damodharan DILLIKANNAN [3,*], S. D. SEKAR [4]

[1] *Department of Mechatronics Engineering, Agni College of Technology, Chennai, Tamil Nadu, India.*
[2] *Department of Mechanical Engineering, Govt. College of Engineering, Salem Tamil Nadu, India (Deputed from Annamalai University),*
[3] *Department of Mechanical Engineering, Jeppiaar Engineering College, Chennai, Tamil Nadu, India.*
[4] *Department of Mechanical Engineering, R.M.K. Engineering College, Chennai, Tamil Nadu, India.*

A R T I C L E I N F O

2025, vol. 45, no.2, pp. 272-284

doi: 10.47480/isibted.1642863

Research Article
Received: 21 February 2025
Accepted: 22 April 2025

* *Corresponding Author*
e-mail: damumech07@gmail.com

Keywords:
ternary blends
fuel injection pressure
EGR; emissions
performance
machine learning optimization

ORCID Numbers in author order:
0000-0002-8923-6831
0000-0003-4741-4860
0000-0002-8804-6913
0000-0000-0000-0000

A B S T R A C T

Modern society prioritizes Sustainable Development Goals (SDGs 7 and 13) to address the fuel requirements of transportation and agriculture, concentrating on clean energy and climate change mitigation. This study examines the combination of Simmondsia chinensis (jojoba) biodiesel and methyl acetate (MA) to improve combustion efficiency and decrease emissions in a Common Rail Direct Injection (CRDi) engine. The ternary test fuels comprised diesel, biodiesel (SCB), and MA additives, formulated as DB50 (50% diesel + 50% biodiesel), DBMA10 (50% diesel + 40% biodiesel + 10% MA), and DBMA20 (50% diesel + 30% biodiesel + 20% MA). Tests performed at 21º CA for fuel injection time, with varied fuel injection pressures (FIP: 400, 500, 600 bar) and exhaust gas recirculation (EGR: 0, 10, 20%), demonstrated that DBMA20 enhanced brake thermal efficiency by 1.02% relative to DB50. NOx emissions decreased by 32.3% and 18.23% in DB50 relative to diesel at 400 bar fuel injection pressure and 20% exhaust gas recirculation. DBMA20 elevated smoke opacity and CO, HC emissions while decreasing FIP and augmenting EGR. Secondly, nonlinear test results and repetitive engine testing make improving IC engine performance with alternate fuels difficult. This challenge is solved using generalisable machine learning models and engine variable optimisation. Machine learning-based long-short-term memory (LSTM) models anticipate and optimise a CRDi engine that runs on ternary test fuel with various injection strategies for FIP and EGR experimental data as an input. This model accurately predicts thermal efficiency, fuel consumption, NO_x, HC, CO, and smoke opacity. LSTM predicted R^2 values of 0.91-0.991, with an MRE of 1%-5%. Best CRDi engine configuration: DBMA20 @ 600 bar FIP, 10% EGR. LSTM improves R^2 and reduces MRE to enhance engine performance. An R^2 value close to 1 is expected. It can conclude that the machine learning based forecasting method is an effective tool for assessing the in depth engine operation relation among input variables.

Dizel Motorlarda Isıl Verimliliğin Optimizasyonu: LSTM Makine Öğrenimi Kullanılarak Üçlü Karışımlar, Değişken Enjeksiyon Basınçları ve EGR ile Performans Tahmini

M A K A L E B İ L G İ S İ

Anahtar Kelimeler:
Üçlü karışımlar
Yakıt enjeksiyon basıncı
EGR; emisyonlar
Performans
Makine öğrenimi optimizasyonu

Ö Z E T

Modern toplum, ulaşım ve tarım sektörlerinin yakıt gereksinimlerini karşılamak amacıyla Sürdürülebilir Kalkınma Amaçları (SKA 7 ve 13) doğrultusunda temiz enerji ve iklim değişikliğiyle mücadeleye odaklanmaktadır. Bu çalışma, Simmondsia chinensis (jojoba) biyodizeli ve metil asetat (MA) karışımının Common Rail Doğrudan Enjeksiyonlu (CRDi) motorda yanma verimi ve emisyonlara etkisini incelemektedir. Üçlü test yakıtları DB50 (50% dizel + 50% biyodizel), DBMA10 (50% dizel + 40% biyodizel + 10% MA) ve DBMA20 (50% dizel + 30% biyodizel + 20% MA) olarak hazırlanmıştır. Deneyler 21° CA enjeksiyon avansında, değişken enjeksiyon basınçları (FIP: 400, 500, 600 bar) ve egzoz gazı resirkülasyonu oranları (EGR: 0, 10, 20%) ile yürütülmüştür. Sonuçlara göre DBMA20, DB50'ye kıyasla fren termal verimini %1,02 artırmış, 400 bar FIP ve %20 EGR koşullarında NO_x emisyonları dizel yakıta göre sırasıyla %32,3 ve %18,23 azalmıştır. Ancak DBMA20, artan EGR ve azalan FIP ile duman opaklığı, CO ve HC emisyonlarını yükseltmiştir. Alternatif yakıtlarla içten yanmalı motor performansını geliştirmedeki doğrusal olmayan deneysel zorluklar, makine öğrenmesi tabanlı Uzun-Kısa Süreli Bellek (LSTM) modeliyle aşılmıştır. LSTM modeli, farklı FIP ve EGR değerleriyle elde edilen deneysel verileri kullanarak termal verim, yakıt tüketimi, NO_x, HC, CO ve duman opaklığını yüksek doğrulukla tahmin etmiştir. Model, R^2 = 0,91–0,991 ve MRE = %1–5 aralığında sonuçlar vermiş; en uygun konfigürasyon DBMA20 @ 600 bar FIP, %10 EGR olarak belirlenmiştir. LSTM'nin yüksek R^2 değeri, yöntemin motor parametreleri arasındaki ilişkileri doğru biçimde modellediğini göstermektedir.

SEMBOLLER / NOMENCLATURE

ASTM	American Society for Testing and Materials
TDC	Top Dead Centre, CA
BSFC	Brake Specific Fuel Consumption (kg/kW-hr)
BTE	Brake Thermal Efficiency, %
CA	Crank Angle, deg
CCI (CN)	Calculated Cetane Index
CO	Carbon monoxide, % vol.
CR	Compression ratio
FIP	Fuel Injection Pressure(bar)
CRDI	Common Rail Direct Injection
SCB	Simmondsia Chinensis Biodiesel
MA	Methyl Acetate (99.6% pure)
DB50	Diesel-50%, SCB-50%
DBMA10	Diesel-40%, SCB-50% + MA10%
DBMA20	Diesel-40%, SCB-50% + MA20%
ECU	Electronic Control Unit
HC	Hydrocarbons, ppm
HRR	Heat Release Rate, J/deg
PCP	Peak Cylinder Pressure, bar
NOx	Nitrogen oxides, ppm
PPM	Parts Per Million
CV	Calorific Value (MJ/kg)
LSTM	Long Short-Term Memory
R2	Correlation Coefficient
MRE	Mean Relative Error
RNN	Recurrent Neural Network
ANN	Artificial Neural Network

INTRODUCTION

Energy plays a crucial role in ensuring a nation's sustainable economic development and is essential for the basic needs of individuals (Mohanrajhu N et al., 2024). To meet the growing energy demand, a substantial amount of energy must be generated and distributed across various sectors, including transportation, domestic use, agriculture, and heavy industry (Babu A et al., 2024). The increasing percentage of energy usage has led researchers to examine ongoing, sustainable, and renewable resources (Jayabal, R et al., 2024). Diesel engines are widely used in transportation due to their superior fuel conversion efficiency (Qiu et al., 2025). However, their higher emission levels are a concern due to adverse effects on human health and the environment. Prolonged exposure to particulate matter increases the risk of respiratory illnesses, including pulmonary cancer (Damodharan, D., et al. 2018). Compression ignition (CI) engines can be operated using a variety of fuels through different methods and modifications (Kannan, R et al., 2024). Reports indicate that the oil obtained from the seeds of the Jojoba tree, known as Simmondsia Chinensis, may grow to an altitude of 1–5 meters and boast a long, long-life expectancy of 150 years (Vellaiyan et al., 2025b). There are several other names for this widely distributed plant in the United States. The oil and wax content of its seeds varies between 44 and 56%. The oil had a beautiful golden hue, was safe for use, and consisted of 97% monoesters, which are long-chain fatty acids and alcohols. This component ensures its stability and ability to withstand extremes of heat, distinguishing it from numerous non-edible oils (Subramanian et al., 2022). When the oil is transesterified, it produces biodiesel with improved properties (Jayabal, et al., 2024). The research study involved a mix of ternary diesel with JME and n-butanol additives. Jojoba oil has a notable n-butanol element (DBJ15), allowing it to generate low-emission varieties in a similar timeframe while maintaining impressive thermal efficiency (Mohanrajhu et al., 2024). It's revealed one of the main issues regarding biodiesel is its vulnerability to oxidative reactions driven by radicals (Li et al., 2025). The high concentration of unsaturated methyl esters makes biodiesel susceptible to oxidation. It requires thoughtful actions, which, among a few others, include the incorporation of protective ingredients (Vellaiyan et al., 2025a). Synthetic antioxidants like butylated hydroxyanisole and butylated hydroxytoluene performed equally effectively as the PFS extract (Zhou et al., 2024).

The current research confirms the effectiveness of plant extracts abundant in phenolic as powerful ingredients for biodiesel (Shubham J et al., 2021). This work revealed that methyl acetate is largely the agent of choice for glues and adhesives that use low-viscosity systems. Adding methyl acetate to petrol enhances its cetane rating, drivability, concentration, and vapor pressure (Jayabal, R et al., 2024). This study evaluated two chemicals, anisole and methyl acetate, for their potential use as fuel ingredients when combined with gasoline and biofuel. Anisole and methyl acetate, for example, have been demonstrated in experiments to work well as petrol and biofuel compounds. However, NOx and soot emissions can be problematic (Londhe, H., et al.,2019). A second study was carried out with biodiesel from WCO at various FIPs. Compared to clean diesel under similar operating conditions, better FIP reduced BTE (Ramesh, A., et al.,2019). This study shows to eliminate slush deposits and colour deterioration in biodiesel fuels by adding antioxidants. Diesel fuels are notoriously fast turning. Due to rust, 1–3-year storage is unlikely. Pyrogallol, diphenylamine, tert-butylhydroquinone, butylated hydroxyl anisole, and methyl acetate are antioxidants. The survey found TBHQ, PL, and MA to be the best antioxidants. Biodiesel mixing mostly uses these additions to stabilise (M. Vijay Kumar et al.,2018). This research discovers the effect of kapok methyl ester mix diesel engine fuel burns when injected with reactive agents and with holes in the injector. A single-cylinder diesel engine was used to analyze a 40% kapok methyl ester mix. Using a 6-hole nozzle, the tests showed that B40 mixed with 1000 ppm tertiary butyl hydroquinone gave off the most heat (102 J/°CA). Propyl gallate had a minimum BSFC of 0.269 kg/kW h at the lowest load with the B40 mix (Narayanan S et al., 2022). Recently, researchers explored the concept of a three-component blend because of its enhanced stability, cost-effectiveness, and minimal adjustments needed for engine hardware settings. This paper investigates the application of methyl acetate alongside diesel and SCOME. Research on the application of methyl acetate antioxidants in engines has been quite limited. Their capacity to reduce smoke has gained significant attention (Karthikeyan S et al.,2023). According to this study, diesel and Prosopis juliflora oil methyl ester (PJOME) was mixed at 10%, 20%, and 30%. Three parametric CRs (16, 17.5, and 19) and FIP (400, 500, and 600) were used. Recent research has shown that B20 and CR16 with FIP 600 bar increase BTE by 33.21% and lower bsfc by 0.25 kg/kW-hr. PCP is 69.28 bar, NHRR is 79.14 J/deg, and exhaust emissions are 55 ppm UHC, 0.25% CO, 34.33% smoke, and 2401 ppm NOx. UHC, CO, and smoke were lower than other mixes, while BTE and NOx were higher(Ramesh, T et al.,2022). This work specifically utilizes an experimental technique to investigate the influence of adjusting intake pressure (IP) on CI engine factors, using a 20% biodiesel derived from Ceiba pentandra. In comparison to diesel (B0) at 200 bar, the biodiesel mix (B20) with a higher IP (260 pressure) increased BTE (9%), CP (8.5%), and HRR (2%) while reducing BSFC (9%), CO (14%), HC (16%),

and smoke (16%). Lower-rate EGR addresses higher NOx emissions at higher IP (Damodharan, D., et al.2018).

Operating an engine in every possible way and with every fuel type is difficult and expensive (Liu et al., 2025). However, diesel engine production and emission conditions can be predicted using machine learning (ML) techniques such as ANN and LSTM which require much smaller effort and assets (Anping et al., 2025). One distinguishing characteristic of these novel methods is their capacity to understand and anticipate specific results autonomously(Yang, R et al.,2022). They discovered that the MLA versions provided adequate reaction latency for actual management purposes. This made them a quick and accurate way to predict when combustion would start in homogeneously charged CI engines, Because of the linear hypothesis addition (Lee, J et al.,2021). Despite the intriguing effects of ANN on exhaust temperature, the study's extensive usage of starting parameters and the risk of failure due to gradient explosion during training necessitate extra effort spent tuning the hyperparameters. On the other hand, irregular shifts usually define thermal stress; collecting and obtaining this information is needed in various situations for research and forecast. However, only a few aspects are considered, and their interdependencies are not considered. Given the scarcity of ANNs, the LSTM model is being evaluated for use in predictive analysis. The utilization of AI in bioenergy processes is negligible, and also, there is a need for additional research to be conducted on the utilization of machine learning (ML) techniques to improve performance and forecast (Liu, J. et al.,2021). Research, however, shows that ML holds much promise for reducing obstacles to the expansion of the bioenergy sector. The subject of study two machine learning methodologies, K-nearest neighbours (KNN) and support vector machines (SVM), to categorise combustion events in a homogeneous charge compression ignition (HCCI) engine. The research indicated that SVM attained a classification accuracy of 93.5%, whilst KNN acquired an accuracy of 89.2% (Angikath S et al., 2020). This study examined average effective pressure prediction using random forests (RF), ANN, and support vector regression. Machine learning models were trained, evaluated, and tested using verified one-dimensional computation fluid dynamics data. Both SVR and ANN models accurately predicted mean effective pressure, with R^2 values of 0.976, 0.961, and 0.964. The RF model has the lowest training and testing error rates of 5.37 and 7.92 (Amad Hussen et al.,2024). This research predicts compression ignition (CI) engine pollution and performance using machine learning algorithms (MLAs). The R^2 scores of linear regression, support vector regression, neural networks, KNN, polynomial regression, Gaussian processes, relevance vector machines, and deep learning (LSTM) algorithms are 0.928, 0.921, 0.334, 0.951, 0.5, 0.7, and 0.961, respectively, compared to the proposed model. The LSTM deep learning model predicts engine reactions better for the dataset used in this study after assessing numerous metrics. Following the algorithm, the LR, SVM, and NN algorithms trail closely (Subramanian K et al.,2024). This study uses LSTM to forecast exhaust gas emissions using just engine characteristics like intake air temperature, emission gas temperature, and injection timing. Deep learning may be used as a virtual emission sensor since it correlates data without automobile specs or data. Since the complicated environment makes it impossible to evaluate deep learning and road car test data, this study employs a single-cylinder diesel engine. Measure the nitrogen oxide by adjusting injection time and intake air temperature from 0 to 100 °C. Nitrogen oxide is reliably predicted with a significant correlation R^2 of 0.994 with little engine data (Shin, D., et al.,2023). This study revealed that it developed the SVM and LSTM models to estimate unmixed turbofan engine emissions and exergy indicators during takeoff. The data show that LSTM has fewer model errors than SVM. The NO_x emission index is predicted by SVM with R^2 0.929074 and LSTM with R^2 0.954878 (Hakan Aygun et al.,2023).

Furthermore, research has yet to be undertaken into employing an SCB-MA blend in a CRDI research diesel engine while altering the FIPs and EGR rates. The initial objectives of this research were to evaluate the engine characteristics of SCB-MA mixtures in a CRDI research diesel engine with different FIPs (400, 500, and 600 bar) and EGR (0, 10, and 20%). The results were subsequently in contrast with those of traditional diesel operations. In addition, machine learning based LSTM model was employed to predict the performance of common rail direct injection (CRDI) diesel engines in terms of both fuel efficiency and emissions.

TESTING APPARATUS AND METHODOLOGY

Test Fuels

Table 1 presents a comprehensive overview of the salient attributes of pure diesel fuel and biodiesel fuel obtained from the residual seeds of Simmondsia Chinensis plant. The consumption of Simmondsia Chinensis oil in CI engines may lead to injector complications due to the heightened viscosity and density of the oil. Using methyl acetate from Millipore and the transesterification process, SCO was changed to SCB, which has lower viscosity and density. A diesel-biodiesel-methyl acetate combination was made. Combining petrol and biofuel formed the binary mix. DBMA10 included 50% diesel, 40% biodiesel, and 10% methyl acetate. DBMA20 and DB50 are binary mixtures.

Table 1: Characteristics of Test fuel

Properties	Standard	Diesel	SCB	SCB 50	Methyl Acetate (MA)	SCB40+ MA 10%	SCB30+ MA 20%
Kinematic viscosity, 40 °C	ASTM D 445	2.89	5.12	4.01	0.4	3.756	3.51
Density (kg/m³)	ASTM D 1298	832	876	854	932	864	873
CV (MJ/kg)	ASTM D 240	42.5	38.25	40.38	21.5	38.29	36.18
CCI	ASTM D 976	47	51	49.3	-	-	-
Flash point °C	ASTM D 93	69	152	120	10	104.6	98.7

Test setup

Figure 1 illustrates the experimental setup under investigation. The Kirloskar TV1 was used for conducting tests and consisted of a mono cylinder, 4S, VCR-water-cooled system that was associated with a dynamometer. NOx pollutants were quantified with an AVL digas 444N analyser and deplete smoke discharges were evaluated with an AVL 437C smoke meter. A CRDI arrangement was necessary to accomplish the infusion conditions required for assessment. The fuel delivery line was modified to connect to the common rail direct injection system, and an elevated-pressure impeller was subsequently installed in the strainer. This functions as a fuel storage tank. The Nira i7r engine control unit is equipped with a

rail pressure sensor for the purpose of maintaining pressure. Due to the significantly increased injection pressures utilised by CRDI, the initial injector was inadequate, and thus, a 6-hole solenoid-regulated injector was selected as a suitable alternative. The ECU was utilised to modify the initial detectors and effectors to ensure their appropriate functionality. Assuming proper functioning of the engine, it is deemed suitable for diagnostic evaluation. The experimentation engine parameters are described in Table 2.

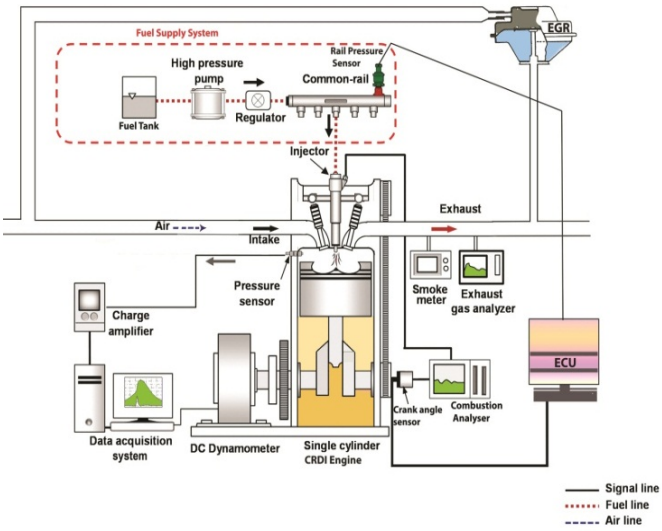

Figure 1. Test engine layout [7]

Table 2. Engine specification

Make and Model	Kirloskar, TV1
Number of cylinders	Single
Stroke	Four
Bore x Stroke length	87.5 mm x 110 mm
Capacity	661cc
Power output	3.5 kW at 1500 rpm
CR	1:17.5
Cooling method	Water-cooled
IT, CA bTDC	23°
FIP	200 to 600 bar

Error Analysis

An instrument's assessment outcomes can be standardized by several test conditions, such as how the test is set up, what reports are made, and the environment. To determine the accuracy of the experiments, it is important to do an uncertainty analysis (Venu, H et al.,2019). Each instrument's process and calibrations are calculated routinely across 5 repeats (n=5). The instrumental uncertainty for each parameter is related to the experiment's uncertainty. In equation (1), the quadratic summation of every extensive parameter with the result of every sample is summed.

$$\sigma x^2 = \sqrt{(Bx^2 + Rx^2)} \quad (1)$$

R_X denotes the density function of errors in repetition. To put it another way, B_X represents the cumulative ambiguity density function. Various tests were run on the analysis results to calculate the null hypothesis. Table 3 lists the instrument's Accuracy, resolution, and range.

Table 3: Instrument's Accuracy, resolution, and range

Measured quantity	Accuracy	Resolution	Range
NOx	±5 ppm	1 ppm vol.	0-5000 ppm
Smoke	±1 %	0.1 %	0-100 %
CO	±0.02 %	0.01 % vol	0-15 %
HC	±10 ppm	1 ppm vol.	0-30000 ppm
CO_2	±0.3 %	0.01 %vol	0-20 %
Oil temperature	±4 °C	1 °C	0-125 °C
Speed	±1 min^{-1}	1 min^{-1}	400...6000 min^{-1}

EGR Setup

The exhaust gas recirculation (EGR) method drops the temperature of the cylinder's charge and the overall temperature, thereby decreasing nitrogen oxide (NO_X) emissions. This also renders EGR denser, resulting in a total rise in its volume. The EGR cooler directs a part of the exhaust gas into the air intake. The exhaust gas recirculation cooler's H_2O functions as a heat exchanger, collecting heat from the retained exit gases. The outlet's temperature must drop by 36 °C during this process. The EGR valve controls the amount of air that circulates inside the engine. The EGR is determined by the orifice dimension. Directing the recycled exhaust gas to the input port was the best approach to start the process. The EGR rate was calculated using equation (2).

$$EGR\% = \left[\frac{(CO_2)_{intake}}{(CO_2)_{exhaust}}\right] \times 100 \quad (2)$$

The AVL 444 N gas apparatus was utilised to ascertain the quantity of CO_2 emitted by adjusting the outlet discharge till the entering carbon dioxide reached a predetermined level (Kim H Y et al.,2019).

Experimental procedure

To explore the potential of replacing 50% of diesel with biodiesel, emissions, efficiency, and combustion properties were analysed. A 50:50 diesel–biodiesel binary blend was prepared and tested, which resulted in higher smoke emissions compared to conventional diesel, thereby affecting performance. As a mitigation strategy, the use of antioxidant additives, a commonly recommended method, was adopted to reduce tailpipe smoke emissions below those of standard diesel engines. The present research selected methyl acetate as an oxidant due to its attributes being comparable to those of low-viscosity substances. The study established a specific diesel volume to meet the objective of substituting 50% of the diesel volume with alternative fuel. Quantity reduced the biodiesel proportion to 20% and supplemented it with the methyl acetate additive. The engine was operated under its standard settings using a ternary blend consisting of 50% diesel, 40% SCB, and 10% methyl acetate, as well as a second blend of 50% diesel, 30% SCB, and 20% methyl acetate. The ternary mix operation reduced smoke emissions below the diesel operation while improving combustion characteristics when combined with the binary mix. The ternary blend, however, resulted in higher NOx emissions. Because of this, we did more tests with the ternary blend at full power, changing the FIP to 400, 500, and 600 bar and the EGR to 0%, 10%, and 20% to find the best operating condition for lowering the smoke and nitrogen oxide. The research upheld a consistent CR 19 and an INT 21º bTDC. To ensure uniform findings, three

different tests were conducted on the same day and under similar climate circumstances. The initial evaluations were done by averaging the results and using neat diesel. Samples were examined for four weeks to validate the variant's uniformity. A UV-visible spectrometer was used to validate the variants' uniformity. The gravitational method examined the Simmondsia Chinensis biodiesel supply in diesel. The variants were balanced in the absence of phase estrangement. The evaluation of combustion characteristics was conducted by analysing the cylinder pressure data. To mitigate the effects of frequent variability, it is necessary to utilize a 100-cycle average when calculating the heat release rate (HRR) based on pressure inferences. The temperature of the lubricating oil was maintained within the range of 85 ºC to 90 ºC. Prior to recording the parameters, the procedure was executed in a continuous manner for duration of 10 to 15 minutes.

Machine Learning Algorithm-based LSTM Network

Long-short-term memory (LSTM) is a neural network developed by Hochreiter and Schmidhuber in 1997. The steady evolution of this model has resulted in a comprehensive and well-organised structure (Zhou, R. et al.,2023). In this research, the LSTM is employed to address the expansion and difficulty in updating partial derivatives W during training, as well as the dependence problem at long distances, which are both challenges for the recurrent neural network (RNN). Figure 2 depicts the neural unit's LSTM internal structure. The LSTM extends the RNN structure with three thresholds: logical control units responsible for managing the network's input and output data at a time ti gets one single piece of information as its input, whereas the Long Short Term Memory (LSTM) network receives an entry consisting of three components. The current value of the network's input (X_t) the output value stored in long short term memory from the previous time step (h_{t-1}) and the cell state, from the previous moment (C_{t-1}) The LSTM neural network performs computations based on the cell state (C_t) and the current time steps output (ht). It utilizes a gating system composed of input gates to bring in information, to the cell state at each time step; forgetting gates to decide what information is no longer needed; and output gates to update the current cell state, for prediction purposes in each time step using equations 6 through 10.

$$f_t = \sigma\,(W_f \cdot [h_{t-1}, X_t] + b_f\,), \quad (3)$$

$$i_t = \sigma\,(W_i \cdot [h_{t-1}, X_t] + b_i), \quad (4)$$

$$o_t = \sigma\,(W_o \cdot [h_{t-1}, X_t] + b_o), \quad (5)$$

$$C_t = f_t\, h_{t-1} + i_t \tanh\,(W_C \cdot [h_{t-1}, X_t] + b_c), \quad (6)$$

$$h_t = o_t \tanh(C_t), \quad (7)$$

Here, "x_t" stands for the input, while "f_t," "i_t," and "o_t" refer to the hidden gate, input gate, and output gate, respectively. The statistic "c_t" represents the cellular state at time "t," after the input and hidden gates has been activated. Simultaneously, "ht" represents all potential states of the LSTM unit's output. To activate the LSTM unit, the double tangent function is utilised, while the sigmoid function is represented by the symbol "δ."

Equations show the input weight coefficients as Wxi, Whi, W_{ci}, W_f, W_{hf}, W_{cf}, W_{xc}, W_{hc}, W_{xo}, W_{ho}, and W_{co}. We refer to the offset vectors as b_i, b_f, b_c, and b_o. LSTM models can deliberately retain important information by considering the state of the cell unit and the configuration of three gates: input, hidden, and output. The input gate plays a crucial role in identifying the incoming data and Managing the input at the present position in the sequence. On the other hand, the concealed gate employs the activation function to decide when to discard previous information. The output gate oversees the retention of data as well as the final output.

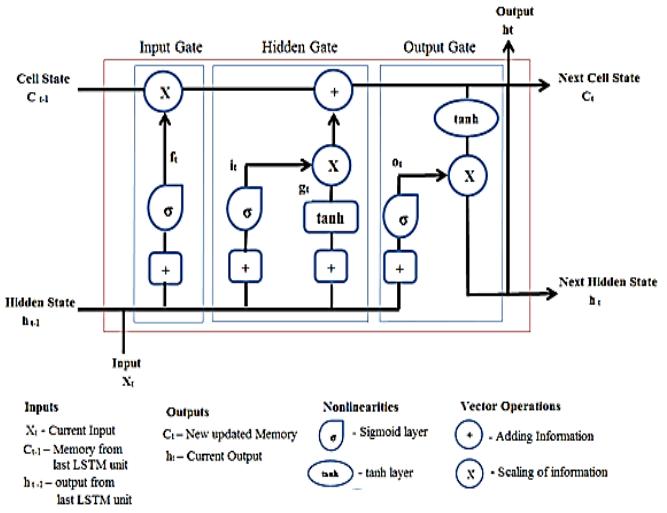

Figure 2. LSTM Architecture

Model Architecture

An LSTM neural network captures temporal relationships in sequential data, which is the heart of our modelling technique. Double-stacked LSTM layers form the model. The first LSTM layer has 100 units and returns sequences for stacking. A second LSTM layer, consisting of 50 units, outputs a fully linked dense layer. LSTM layers are followed by 0.2-dropout layers to prevent overfitting. Signature activation is used in the last dense output layer.

Training and Dataset

This analysis used 298 multivariate time series samples. Each sample has 50 time steps and 10 characteristics that track dynamic system activity. A publicly available benchmark repository utilised in time series modelling studies provided the data. The dataset was extensively preprocessed before training. Linear interpolation was used to fill missing values, and min-max scaling normalized all features to [-1, 1] to ensure consistency and expedite model convergence. With a random seed to assure repeatability, the cleaned data was split into training (80%), validation (10%), and test (10%) groups in fixed proportions.

This error reduction is visible in the high scores earned on both the exercise and training datasets, which are 99.99% and 100%, respectively. These high scores imply that the LSTM model is generalised, with minimal bias and variation. In other words, it performs well on both training and testing data, indicating its capacity to predict accurately on previously unknown data.

Model Hyperparameter Tuning

Hyperparameters affect model behaviour and performance. These settings are tuned to improve model performance. Layers (1, 2, 3, 4), hidden units and epochs (10, 20, 30, 40, 50, 60, 70, 80, 90, 100, 110, 120, 130, 140, 150, 160), and batch size (1, 3, 5, 7, 9, 11, 13, 15) are predefined LSTM hyperparameters. Latin hypercube sampling generates 300

LSTM hyperparameter possibilities. To evaluate LSTM performance with 300 hyperparameter combinations, the calibration set uses a 20% holdout method. Grid Search systematically evaluates these hyperparameters to find the ideal set that improves regression model prediction accuracy. This method avoids the drawbacks of attempting all possibilities and saves time.

Model Evaluation

Regression issues aim to transfer the dependent variable's actual values to the models' anticipated values. Regression model performance may be assessed using measures like R^2 score and MRE. While the R^2 score evaluates model performance, it does not imply inaccuracy. Common regression model goodness-of-fit indicators include the R^2-score, which spans from 0 to 1. A value of 0 shows the model doesn't explain response data variability. However, a score of 1 indicates that the model matches the data flawlessly. The R-squared equation follows.

$$R^2 = 1 - \left(\frac{\sum_{i=1}^{n}(t_i - o_i)^2}{\sum_{i=1}^{n}(o_i)^2}\right) \quad (8)$$

Mean Relative Error (MRE) is a statistic used to assess model predictions, especially for regression tasks with continuous variables. This is similar to Mean Absolute Error (MAE), but the MRE normalizes the difference between anticipated and actual values by the actual values, making it more relative.

$$MRE = \frac{1}{n}\sum_{i=1}^{n}\left|100 \times \frac{(t_i - o_i)}{t_i}\right| \quad (9)$$

RESULTS AND DISCUSSION

COMBUSTİON ANALYSİS

Peak pressure analysis

The variations of peak pressure at maximum load are depicted in Figure 3. The DBMA20 fuel blend produced a higher peak cylinder pressure (PCP) compared to the other tested fuels. The difference is primarily due to its longer ignition delay, which allows for a more uniform air-fuel mixture, leading to a more intense premixed combustion phase and an increase in PCP (Jayabal, R et a., 2025). From the plot, an increase from 400 to 600 bar increases the PCP for the methyl acetate blends. The PCP increased from 80.02 bar to 85.45 bar, 73.52 bar to 76.21 bar, and 73.15 bar to 77.15 bar. However, while EGR levels increased from 0% to 20%, PCP decreased at all FIP levels, from 8.71% at 400 bar, 7.48% at 500 bar, and 10.81% at 600 bar, respectively. Specifically, this occurs because the ignition delay increases as the injection pressure decreases. Lower injection pressures also result in larger fuel droplet sizes, which lead to poorer air-fuel mixing and a subsequent reduction in in-cylinder pressure(Kumar, P. et al.,2018). The PCP of methyl acetate mixtures decreases as EGR rates escalate. This occurs because the inert gases in the redirected exhaust gases serve as heat sinks by absorbing the energy released during combustion. Consequently, the cylinder's maximum pressure is reduced (Ashok, B., et al.,2019).

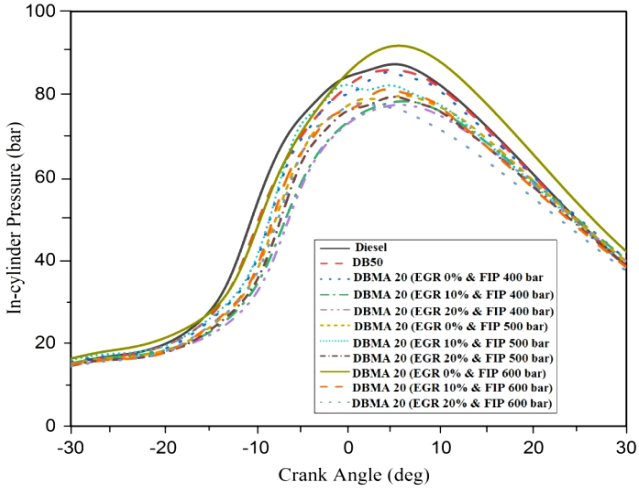

Figure 3. In-cylinder pressure at different FIP and EGR level

Heat release rate

Figure 4 illustrates the variations in heat release rate (HRR) among different test fuels under maximum load conditions. At an injection pressure of 600 bar, the DBMA20 blend showed a higher heat release rate because it took longer to ignite and had more oxygen available. These factors enhance the combustion rate during the process, resulting in elevated HRR levels (Ashok, B., et al. 2019). When the fuel injector pressure is decreased, the HRR slope changes from left to right, and with increasing EGR rates, the arc changes even more. Concerning the 0%, 10%, and 20% values at 400 bar, the heat release rate values are 49.23 J/° to 45.80 J/°, respectively. Similarly, at FIP values of 500 bar and 600 bar, the HRRs are 55.66J/°, to 47.79J/°, and 60.984J/°, to 53.81J/° respectively at EGR rates 0%, 10%, and 20%. Sprayer nozzles have a higher equivalency ratio and impair the air-depletion process, significantly affecting burning and lowering the HRR at reduced rail injector levels(Sharma, et al.,2019). It states that low injection pressure causes minimized HRR peaks. Moreover, a reduced mass fraction at retard injection pressures produces a lower gas temperature and, hence, a minimum HRR. As the EGR rate rises, peak HRR noticeably falls. The presence of polyatomic molecules like CO_2 and H_2O in the exhaust gases dilutes the intake air and increases the specific heat capacity. As a result, the injected fuel undergoes incomplete combustion, leading to a reduction in the HRR(Jaichandar, S et al.,2013).

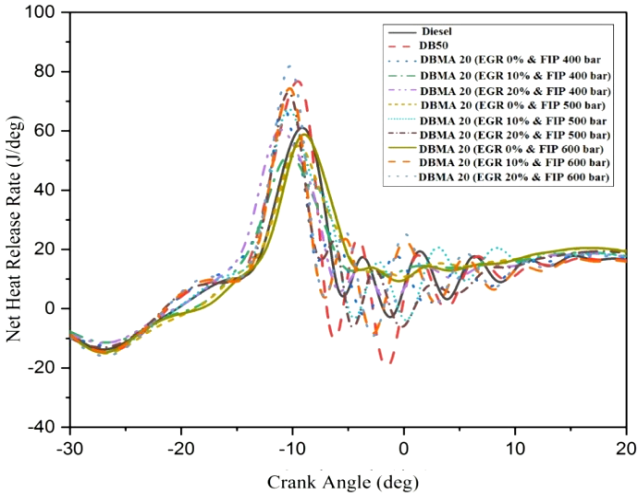

Figure 4. HRR at various FIP and EGR levels

PERFORMANCE ANALYSİS

Brake thermal efficiency

Figure 5 shows FIP and EGR-related brake thermal efficiency (BTE) variations. At rated power and standard engine specifications, diesel, DB50, DBMA10, and DBMA20 had BTE values of 35.87%, 33.91%, 34.7%, and 35.2%. The DBMA20 blend's lower calorific value, improved atomisation, and inherent oxygen content extended the combustion process and increased efficiency, improving BTE by 1.29% over the DB50 blend at 600 bars of injection pressure. The greater cetane index and shorter ignition delay of DBMA20 boosted the BTE marginally, improving engine productivity (Ashok, B., et al.,2019). Using EGR values of 0%, 10%, and 20% at 400 bar, the engine's BTE is 32.1%, 30.5, and 29.14%, respectively. Similarly, at 500 bar and 600 bar FIP, the brake thermal efficiency is 33.8%, 32.33%, 30.71%, 35.2%, 33.63%, and 31.65%, respectively, at EGR rates of 0%, 10%, and 20%. The graph shows that the best BTE for the ternary mix FIP at 600 bars was 1.5% higher than that for a similar EGR level. This improvement is supported by HRR analysis. At 600 pressures, the ternary mix FIP has a more concentrated heat release rate and takes more beneficial work, yielding a greater BTE. As the EGR rises, the ternary blend's BTE diminishes and lack of Exhaust particles burning is led to reducing the BTE (Kim, H. Y, et al. 2019).

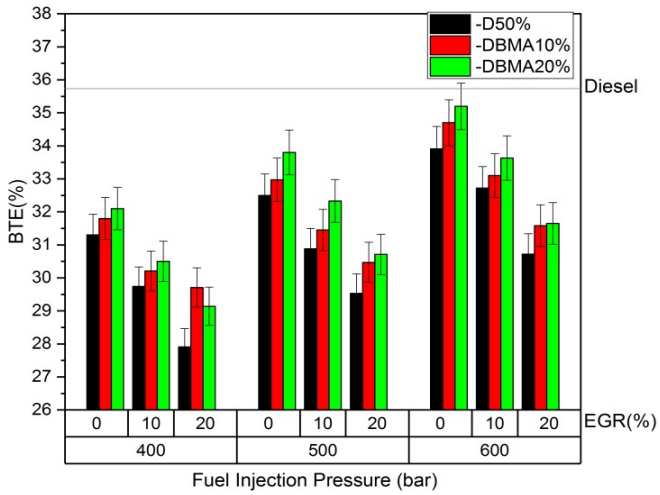

Figure 5. BTE at different FIP and EGR rate

Brake specific fuel consumption

Brake-specific fuel consumption is a quantity that is directly proportional to the volume of injected fuel and the calorific rating. Diesel has a lower BSFC than biodiesel mixtures as a result of its high calorific value and low mass (Sharma et al.,2019). Figure 6 depicts the BSFC of the test variants at various FIP and exhaust gas recirculation values. At the fixed power and engine operating circumstance, the BSFC for Diesel, DB50, DBMA 10 mix, and DBMA 20 blend were determined to be 0.217, 0.26, 0.24, and 0.23 kg/kW-hr, respectively. The correlation between BTE and BSFC is that fuels with a lower BTE will have a higher BSFC. Therefore, the rationale for the variations in BTE across biodiesel, biodiesel-MA blends, and diesel fuel also applies to BSFC (Jayabal, R et al.,2024). The BSFC for the DBMA20 variant was reduced to 600 bar when compared to the DBMA10 blend and was equal to the DB50 blend. This is due to the combined influence of the ternary variant's lower LHV, which necessitates a slightly higher quantity of fuel to produce equivalent energy to split the ternary variant's existing aromatic compounds. It eventually increases the fuel supply, and BSFC decreases (Rangabashiam, D., et al.2020). The drop in BSFC can be seen in the graph when the FIP is increased from 400 to 600 bars. As an illustration, the values decreased from 0.26 to 0.238 kg/kW-hr, 0.289 to 0.267 kg/kW-hr, and 0.31 to 0.286 kg/kW-hr for 0%, 10%, and 20% EGR, respectively. At lower injection pressures, air penetration can be hindered due to larger fuel droplet sizes and a reduced excess air ratio. As a result, BSFC increases and combustion efficiency decreases (Ramachander et al., 2021). In the meantime, increasing the EGR rates will result in a higher BSFC. The BSFC increased from 0.238 to 0.286 kg/kW-hr at a FIP of 600 bars when the EGR level increased from 0% to 20%. Specific heat capacity rises when exhaust gas is induced. The charge slows the flames spread and raises the chance of a malfunction by lowering the cylinder's temperature. As a result, more fuel is required to sustain the ignition, elevating the BSFC (Prasada Rao, G et al.,2021).

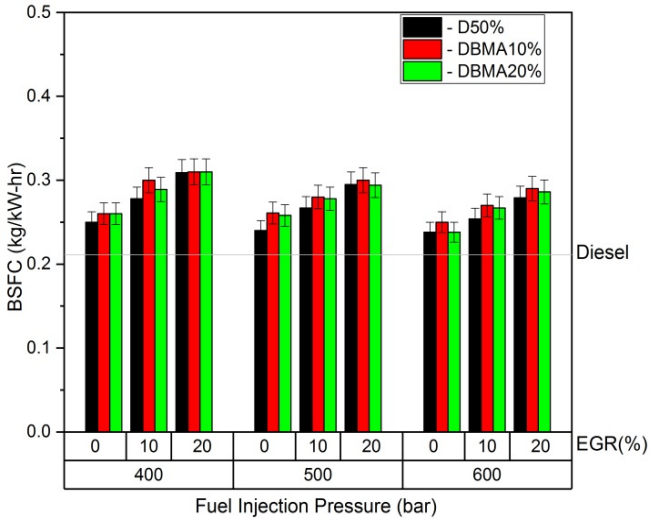

Figure 6. BSFC at various FIP and EGR rate

EXHAUSTS ANALYSİS

Oxides of nitrogen emissions

The combustion temperature, the local air-fuel ratio, and the duration of the combustion process primarily influence NO_x emission levels. The three key parameters that govern NO_x formation are the in-cylinder temperature, the oxygen concentration, and the reaction time (K, S et al.,2020). The disparity of Nox at various FIP and EGR rates for the binary and a ternary blend is revealed in Figure 7. At stated output conditions and engine stock operating, the Nox level for Diesel, DB50, DBMA10 blend, and DBMA20 blend at FIP 600 bar were 2683 ppm, 2162 ppm, 2231 ppm, and 2353 ppm, correspondingly. While contrasted to the binary blend, the tripartite combine emitted more Nox due to the inclusion of elevated methyl acetate, which encourages burning, crowning in higher gas temperature and greater Nox. The DB50 blend is 19.41% less expensive than the reference diesel. Biodiesel exhibits reduced volatility in comparison to diesel fuel, resulting in a slower rate of evaporation. The absence of chemical aromas in biodiesel may be attributed to the observed decrease in Nox emissions (Ahamad Shaik, A., et al.,2020). The methyl acetate additive blend is 5.18% higher Nox than the DB50 blend and 12.14% lower than the reference diesel. The higher temperatures from burning the primary infused charge resulted in the creation of monoatomic N_2, leading to higher NO_x emissions (Mani, M et

al.,2010). Increasing the EGR percentage at a fixed FIP significantly lowered Nox emissions. For instance, at 400 bar FIP, a rise from 0% to 20% EGR resulted in a 32.34 % drop in Nox. This drop was 18.23% at 600 bar FIP with an EGR rate ranging from 0% to 20%. Greater EGR values are responsible for lower Nox pollution. This is because high-heat-capacity inactive entities in the emissions, such as carbon dioxide (CO_2), water vapour (H_2O), and others, consume the heat produced during burning, culminating in a reduced PCP and maximal HRR(Sharbuddin Ali, S. et al.,2020). The plot shows that Increased EGR rates significantly reduced Nox production. At all EGR rates, lower FIP resulted in minimum Nox emissions. For example, DBMA 20 blend was reduced from 2353 to 2068 ppm as the FIP was reduced from 600 to 400 bar at 0% exhaust gas recirculation level. Likewise, it reduced from 2127 to 1749 ppm and 1924 to 1400 ppm at 10% and 20% EGR levels, respectively. The combustion process experiences insufficient fuel atomization at lower injection pressures, which leads to reduced HRR. Furthermore, as the injection pressure decreases, a smaller mass fraction of fuel is burnt, resulting in reduced NO_x emissions due to the corresponding decrease in gas temperature(Fayad, M.A et al.,2019).

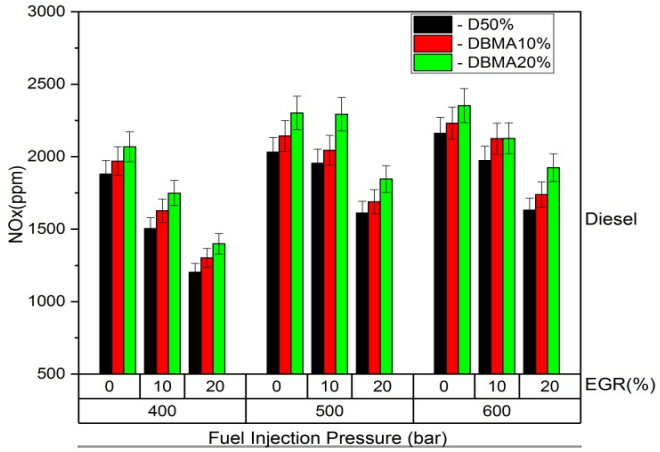

Figure 7. Nox emissions at different FIT and EGR levels

Smoke opacity

Smoke opacity indicates incomplete combustion and excessive tailpipe particulates. Oxygen deficit, in-cylinder temperature, fuel characteristics, and combustion efficiency affect it. Poor atomisation or delayed ignition can increase smoke opacity (Venu, H et al.,2019). The tested fuels SO at different FIP and exhaust gas recirculation at maximum power is illustrated in Figure 8. 58.6% and 48.7% for DB50 and diesel blends exhibit the highest smoke opacity among the methyl acetate blends. Compared with the binary variant, the smoke opacity declined considerably under the ternary blend. It is primarily due to improved fuel atomisation and combustion efficiency, leading to more complete burning of the fuel while also reducing smoke emissions (Rangabashiam, D., et al.,2020). It can be revealed that the smoke opacity15.2% dropped at FIP and rose from 400 to 600 bar at all exhaust gas recirculation levels. It was because of the high surplus air correlation that the evaporation procedure was successful. As a result, there were fewer fuel drops. A limited volume of smoke constituted the central area(Shrivastava, P et al.,2020). The smoke opacity increases when the EGR level is raised at similar fuel injection pressure. DBMA20 at 600 bar smoke opacity rose from 28.3% to 41.6 % when the EGR level was elevated from 0% to 20%. At a fuel injection pressure of 500 bar, it rose from 30% to 43.5%, and at a FIP of 400 bar, it rose from 32.6% to 45.7. EGR reduces the cylinder temperature by absorbing heat, which slows fuel vaporization and promotes smoke formation in rich zones. It also hinders ignition delay by diluting oxygen levels(Zhou, X., et al.,2020). Therefore, low smoke emissions were produced at a higher FIP.

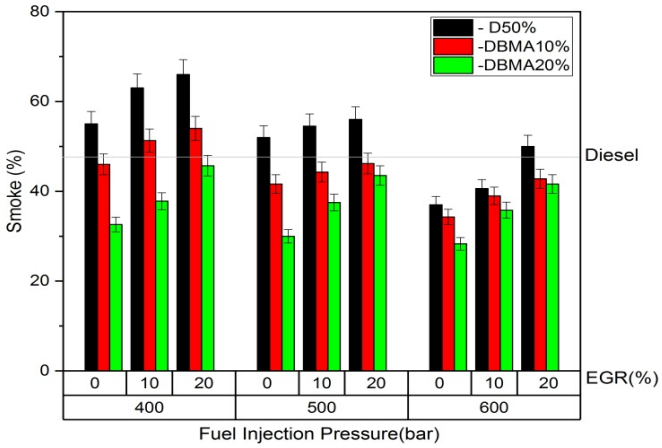

Figure 8. Smoke opacity at different FIT and EGR levels

Carbon monoxide emissions

The disparities at different FIP and EGR levels for the test blends are portrayed in Figure 9. At the rated power output and engine stock Settings, the carbon monoxide level for Diesel, DB50, DBMA10, and the DBMA20 at 600 bar was found to be 1.052%, 0.341%, 0.238%, and 0.183% by volume, respectively. In contrast to the DB 50 blend, Methyl acetate in the diesel/SCB blend substantially reduced CO emission. This is because the oxygen content in the ternary blend can enhance combustion efficiency, thereby promoting the conversion of CO to CO_2 (Londhe, H., et al.,2019). The carbon monoxide reduced as the FIP dropped from 600 to 400 bar at all exhaust gas recirculation levels, for example, DBMA20 blend 0.23 to 0.18% vol. at 0% EGR, similarly 0.48 to 0.31% vol. at 10% and 0.66 to 0.42 % vol. at 20% EGR levels. Diminished FIPs minimise the potential of CO levels due to less exterior wettability and fuel buildup in crevices (Jayabal, R et al.,2024). CO emissions increase as exhaust gas recirculation levels increase across all fuel injection pressures. Results showed that CO exhaust was 0.23% vol., 0.48% vol., and 0.66% vol. when EGR rates of 0%, 10%, and 20% were considered at FIP 600 bar, accordingly. Similarly, at a FIP of 500 bar and 400 bar, the CO discharge was 0.22% vol., 0.39% vol., 0.59 % vol. and 0.18% vol., 0.314% vol., 0.42% vol., respectively at EGR rates of 0%, 10%, and 20%. The EGR diminishes the oxygen supply for combustion. which can lead to incomplete burning of the fuel and increased CO formation. Additionally, the reduced combustion temperature resulting by EGR inhibits the oxidation of CO to CO_2, hence increasing CO emissions (Ahamad Shaik, A., et al.,2020).

Hydrocarbon emissions

Hydrocarbon (HC) emissions were elevated due to incomplete combustion and flame quench. The A/F proportions and cetane index are the primary factors that impact HC levels (Ramachander et al., 2021). All the FIP and EGR combination test results for hydrocarbon levels

are shown in Figure 10. Under normal engine conditions and rated power output, we found 80.6 ppm of hazardous emissions for diesel at 600 bars, 53 ppm for DB50, 50.4 ppm for DBMA 10 mix, and 48 ppm for DBMA 20 blend.

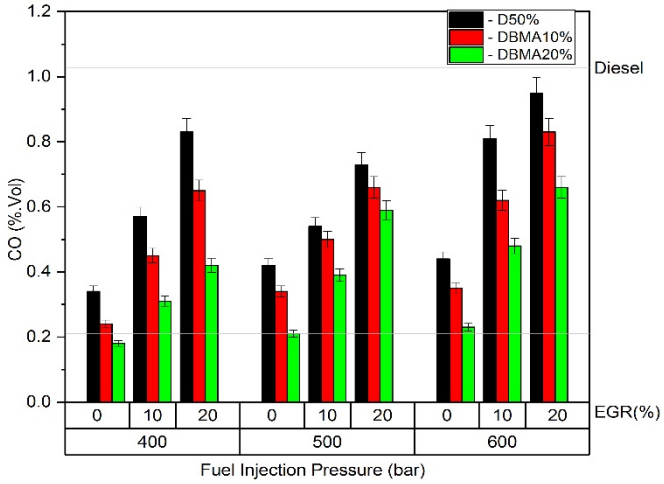

Figure 9. CO emissions at different FIT and EGR levels

This clearly shows a reduction in the use of HC under the ternary variant. Biodiesel exhibits lower HC emissions compared to diesel due to higher combustion temperature resulting from the increased oxygen content in the fuel (Ramesh, T et al.,2022). From the plot, a noticeable HC emission diminishes across the FIP reduced from 600 to 400 bar at all the exhaust gas recirculation levels. For instance, DBMA20 blends 48 ppm to 39 ppm at 0% EGR, 59.4 ppm to 49.5 ppm at 10% EGR, and 70.2 ppm to 58 ppm at 20% EGR levels, respectively. In other terms, a greater FIP is associated with a rise in HC emissions. The droplet size diminishes and the velocity increases. This results in elevated UBHC emissions due to the incomplete combustion of fuel droplets (Chen, Y., et al.,2020). At FIP 600 bar, the HC emits were 48, 59.4, and 70.2 ppm, respectively, with EGR ratios of 0%, 10%, and 20%. Likewise, with a FIP of 500 bar and 400 bar, the HC emits were 41 ppm, 52.2 ppm, and 60.3 ppm; 39.5 ppm, 49.5 ppm, and 58 ppm, correspondingly, when the EGR rates were 0%, 10%, and 20%. Reducing the fuel injector pressure from 600 to 400 bar while maintaining an EGR rate of 10% results in a 16.6% reduction in HC emissions. The phenomenon was attributed to delayed fuel injection, which increased the likelihood of fuel impingement and accumulation in confined regions with limited combustion efficiency, thereby resulting in the presence of unburned or partially oxidized compounds (Fayad, M.A., et al., 2019).

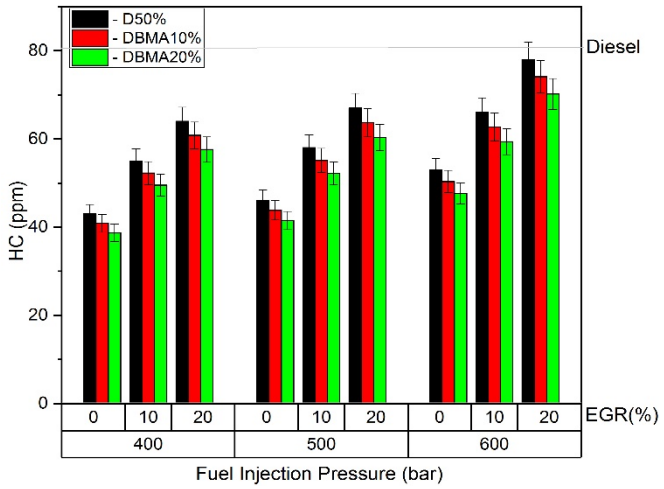

Figure 10. HC emissions at various FIT and EGR rate

The experimentation reveals that the DBMA20 at 600 bar with EGR 10% shows the best results in functionality and CRDI outputs. So, the LSTM-based machine learning approach is used to predict and validate physical experimentation accuracy.

LONG – SHORT TERM MEMORY (LSTM) MODEL

In the second phase of this research, a Long Short-Term Memory (LSTM) model was developed to predict diesel engine performance characteristics based on experimental results. The input factors were FIP, biodiesel proportion, and EGR, while the results measured were BTE, BSFC, NO_x, HC, and CO. Microsoft Excel was used to record the experimental data. CO, HC, smoking, NO, and BTE were considered predictor variables. Approximately 298 individual experiments were conducted using various combinations of input parameters. After data processing and LSTM model training, the optimal input feature values were identified.

The procedure followed to determine the best value is shown in Figure 11. The flowchart begins with experimental data collecting on diesel engine combustion, performance, and emission characteristics. After data collection, a machine learning method is chosen based on the issue and dataset. The next stage is to utilise cross-validation to split the dataset into training and testing sets, using 80% for model training and 20% for testing. The training data is used to create a prediction model using the chosen machine learning method. The model is validated using testing data and rated based on a squared correlation coefficient (R^2) better than 0.9. We iteratively retrain the model if it misses certain validation levels to improve accuracy. Predictions are made using new input data after model validation. The trained machine learning model properly predicts engine performance and emissions in the final stage.

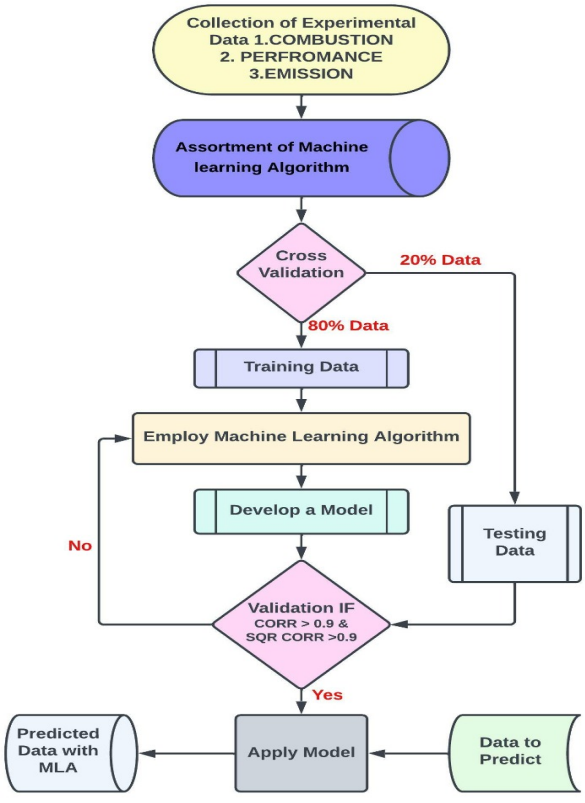

Figure 11. LSTM-based Machine Learning Algorithm model

Each experimental value is recorded by hand, which introduces the possibility of human error. The entire dataset is preprocessed before any simulation is done to normalize the numbers for the following ML computations. A correlation analysis can be employed to ascertain the degree of linearity in the association between the predictor and respondent variables. The correlation coefficient is used to ascertain the degree of association between each independent variable and its corresponding dependent variable. The correlation values range from -1 to 1, which shows that the correlation can be either negative or positive. The degree of association between the input and output features is characterized by a low correlation coefficient, which ranges from -1 to +1. This means that methods that work well with nonlinear models should be used. The data set is split into 80 percent for use in training and 20 percent for testing. The division is conducted randomly to avoid favoritism in the selection of instances. Figure 12 (a) shows the 3D models' disparities of LSTM-oriented functionality and exhaust productions, and Figure 12 (b) shows the 2D Linear Fit Variation of LSTM-based performance and exhaust outputs.

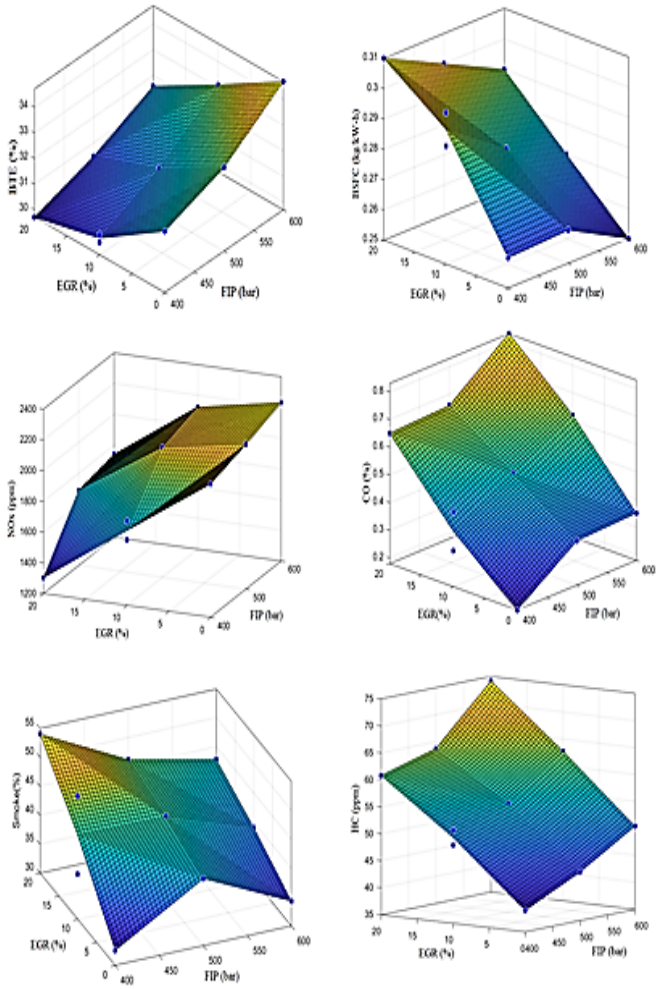

Figure 12. (a) 3D models disparities of LSTM-oriented functionality and Exhaust productions

The predicted and discussed outcomes for BTE and BSFC are shown in Figures 13 (a) and (b). It was found that the R^2 values were 0.9619 and 0.9509. The output of the replicated LSTM demonstrates its capacity to forecast significant aspects. The MRE values for the strategies above are 1.82 and 1.57 percent. The values of R^2 for NOx, CO, smoke, and HC in comparison of predicted and actual findings were 0.9965, 0.9125, 0.9835, and 0.9879, respectively. As per the outcomes of the LSTM-based model, MLA is adequate for estimating output pollutants such as NOx, CO, smoke, and HC. The maximum allowable concentrations (MRE) of NOx, CO, smoke, and HC are 3.04%, 5.87%, 2.44%, and 1.68%, respectively. Table 4 shows an overview of the estimated values.

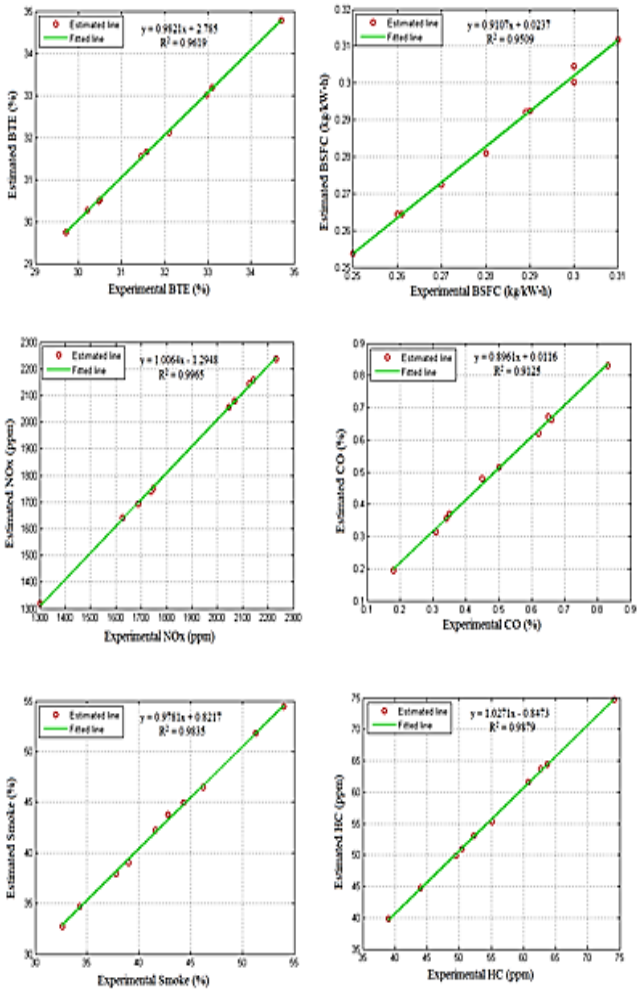

Figure 12. (b) 2D Linear Fit Variation of LSTM-based Performance and Exhaust outputs

LSTM Verifications

The viability of the applied approach must be verified before it can be used. The LSTM was used to develop enhanced engine operating parameters, which were then used in experiments. The algorithm produced the expected significances from the replications with the failure periods (10) and displayed them in Table 5 for the corroboration evaluation.

$$\text{Error } (\%) = \frac{\text{Real Value} - \text{Forecast Value}}{\text{Real Value}} \; x \; 100 \qquad (10)$$

Table 4. Estimate the evaluation engine's LSTM-oriented functionality

Evolution factors	MRE (%)	R^2
BTE (%)	1.82	0.9619
BSFC (kg/kW-h)	1.57	0.9509
NOx (ppm)	3.04	0.9965
Smoke (%)	2.44	0.9125
HC (ppm)	1.68	0.9835
CO (%)	5.87	0.9879

Verification is needed to get the best outcomes. Due to the preservation of two tests, the mean value was calculated at the maximum input variable, considering the LSTM's EGR, DBMA%, and variable fuel injection pressure (FIP)

requirements. The equation has an error rate ranging from 5.88% at its highest to 0.13% at its lowest. It was demonstrated that the overall errors in efficiency and emission forecasts were less than 6%.

Table 5. Verification of the anticipated and actual values

Ternary Fuel Proportion (%)	Load (%)	Fuel Injection Pressure (bar)	EGR (%)	Value	BTE (%)		BSFC (kg/kw-h)	
				Predicated	34.83		0.261	
				Observed	33.63		0.267	
				Error (%)	3.44		2.24	
DBMA20	100	600	10		NOx (ppm)	HC (ppm)	CO (%)	Smoke (%)
				Predicated	2124.3	61.3	0.51	35.2
				Observed	2127	59.4	0.48	35.8
				Error (%)	0.13	3.09	5.88	1.67

The LSTM is an excellent way to determine how the different parameters affect each other. Therefore, LSTM was an effective instrument for forecasting the characteristics of diesel engines. MLAs can forecast operational factors and pollution pollutants, but the complexity and diversity of the problem may cause other quantitative and computational techniques to fail.

CONCLUSION

This study aims to investigate the interaction between the FIP and EGR values and how they affect the variation of engine parameters in several SCB-MA blend combinations. The most important findings are outlined in the following summary.

- The cylinder pressure and HRR decreased for all variants when the EGR rate was raised, and the IP was lowered.
- The DBMA20% blend, at FIP 600 bar with EGR10% rates, achieved 1.02% and 0.53% improved BTE compared to the DB50 and DBMA10 blends. However, compared to the DBMA20 blend, the BTE was marginally less than the reference diesel.
- Because of decreased FIP and increased EGR rates, reduced NOx emissions were observed. The study reveals that the utilization of DB50 resulted in a significant reduction of NOx emissions by 32.3% compared to neat diesel. Additionally, the reduction in NOx emissions was observed to be 18.23% higher at FIP 400 bar with EGR by 20%.
- The DBMA20 blend increased smoke opacity by 28.3% and 41.6% at 600 bar FIP with EGR 10 and 20% compared to DB50 and DMA10%
- The levels of HC and CO emissions exhibited an increase across all Fuel Injection Pressure (FIP) settings and elevated Exhaust Gas Recirculation (EGR) rates.
- Machine learning was enough to predict the CRDi engine outcome variants for different test blends. The BTE, BSFC, NOx emissions, HC emissions, and CO emissions R^2 values were close to 1. When the MLA analyzed the experimental data, a close correlation was found between expected and actual outcomes.

The DBMA20 blend operated at FIP 600 bar, and 10% EGR enhanced performance and reduced emissions when correlated with the other injection pressures and EGR rate operations. The results indicate that the utilization of Simmondsia Chinensis seed biodiesel blend, containing 20% by volume of DBMA, can be effectively employed in CRDI diesel engine applications, resulting in decreased emissions, as supported by both experimental and predictive data.

FUTURE SCOPE

Future research can produce adaptive, self-learning LSTM models that dynamically adjust to engine conditions to improve performance and operating flexibility. This strategy might also improve fuel economy and pollution compliance in large-scale engine operations, addressing environmental issues.

STATEMENTS

Karthikeyan Subramanian: Methodology, Interpretation, Conducted the experiments, writing manuscript. Sathiyagnanam Amudhavalli Paramasivam: supervision, Damodharan Dillikannan: Investigation, Resource, S. D. Sekar: Project administration.

REFERENCES

Ahamad Shaik, A., et al.,(2020), Combined influence of compression ratio and EGR on diverse characteristics of a research diesel engine fueled with waste mango seed biodiesel blend. Energy Sources, Part A: Recovery, Utilization, and Environmental Effects, p. 1-24. https://doi.org/10.1080/15567036.2020.181180

Amad Hussen, Tanveer Alam Munshi, Labiba Nusrat Jahan, Mahamudul Hashan, (2024) Advanced machine learning approaches for predicting permeability in reservoir zones based on core analyses, Heliyon, Volume 10, Issue 12, e32666,https://doi.org/10.1016/j.heliyon.2024.e32666.

Angikath Shamsudheen, F., Yalamanchi, K., Yoo, K., Voice, A. et al.,(2020) "Machine Learning Techniques for Classification of Combustion Events under Homogeneous Charge Compression Ignition (HCCI) Conditions," SAE Paper 2020-01-2020, https://doi.org/10.4271/2020-01-1132.

Anping, W., Hua, Z., Al-Bukhaiti, K., Cheng, X., Ji, X., Wang, J, Shan, T. (2025). Bayesian-Driven Optimization of MDCNN-LSTM-RSA: A New Model for Predicting Aeroengine RUL. IEEE Transactions on Reliability, 1-12. https://doi.org/10.1109/TR.2025.3574975

Ashok, B., et al., An investigation on CI engine characteristics using pork lard methyl ester at various injection pressures and injection timings. International Journal of Green Energy, 2019. 16(11): p. 834-846. https://doi.org/10.1080/15435075.2019.1641107

Ashok, B., et al.,(2019), Comparative assessment of hexanol and decanol as oxygenated additives with calophyllum inophyllum biodiesel. Energy, 173: p. 494-510. https://doi.org/10.1016/j.energy.2019.02.077

Babu Aurtherson P, Dinesh Babu Munuswamy, Ravikumar Jayabal, Yuvarajan Devarajan.(2024), Performance and Emission Characteristics of a CRDI Diesel Engine Fuelled by SiO2 Nanoparticle-Waste Fat Biodiesel Blends J. China Petroleum Processing & Petrochemical Technology, 26(1): 56-66. https://www.ivysci.com/en/articles/8548285

Y Chen, et al.,(2020) Study of injection pressure couple with EGR on combustion performance and emissions of natural gas-diesel dual-fuel engine. Fuel, 261: p. 116409. https://doi.org/10.1016/j.fuel.2019.116409

Damodharan, D., et al.,(2018), Cleaner emissions from a DI diesel engine fueled with waste plastic oil derived from municipal solid waste under the influence of n-pentanol

addition, cold EGR, and injection timing. Environmental Science and Pollution Research, 25(14): p. 13611-13625. https://doi.org/10.1007/s11356-018-1558-5

Damodharan, D., et al.,(2018), Combined influence of injection timing and EGR on combustion, performance and emissions of DI diesel engine fueled with neat waste plastic oil. Energy Conversion and Management, 161: p. 294-305. https://doi.org/10.1016/j.enconman.2018.01.04

Fayad, M.A.,(2019), Effect of renewable fuel and injection strategies on combustion characteristics and gaseous emissions in diesel engines. Energy Sources, Part A: Recovery, Utilization, and Environmental Effects, 42(4): p.460-470. https://doi.org/10.1080/15567036.2019.158709

Hakan Aygun, Omer Osman Dursun, Suat Toraman, (2023) Machine learning based approach for forecasting parameters of mixed flow turbofan engine at high modes, Energy, 271 , 127026, https://doi.org/10.1016/j.energy.2023.127026.

J. Ramachander, S.K. Gugulothu, G.R.K. Sastry, Jibitesh Kumar Panda, M. Siva Surya,Performance and emission predictions of a CRDI engine powered with diesel fuel: A combined study of injection parameters variation and Box-Behnken response surface methodology based optimization,Fuel,290,2021, https://doi.org/10.1016/j.fuel.2020.120069.

Jaichandar, S. and K. Annamalai,(2013), Combined impact of injection pressure and combustion chamber geometry on the performance of a biodiesel fueled diesel engine. Energy, 55, Pp:330-339. https://doi.org/10.1016/j.energy.2013.04.019

Jayabal, R. (2024). Advancements in catalysts, process intensification, and feedstock utilization for sustainable biodiesel production. Results in Engineering, 24, 103668. https://doi.org/10.1016/j.rineng.2024.103668

Jayabal, R. (2025). Environmental and energy impacts of lychee seed biodiesel blends with acetylene fumigation in a dual-fuel diesel engine. Results in Engineering, 25, 103659. https://doi.org/10.1016/j.rineng.2024.103659.

Jayabal, Ravikumar, and S. Madhu.(2024) "Assessment of Emission Reductions in a Diesel Engine Using Graphene Oxide Nanoparticle-Muskmelon Waste Seed Biodiesel Blends." SAE Technical Paper Series 1. https://doi.org/10.4271/2024-01-5240.

Jayabal, Ravikumar, G. M. Lionus Leo, and S. Madhu.(2024), "Assessing the Engine Performance of Rubber Seed Oil Biodiesel Blends in Compression Ignition." SAE Technical Paper Series 1. https://doi.org/10.4271/2024-01-5228.

Jayabal, Ravikumar, G.M. Lionus Leo, M. Chrispin Das, S. Sekar, and S. Arivazhagan.(2024), "Impact of Ammonia Energy Fraction on Improving Thermal Efficiency and Emissions of Ammonia/ Biodiesel in Dual Fuel Diesel Engine." Process Safety and Environmental Protection 188 1398–1410. https://doi.org/10.1016/j.psep.2024.06.016.

Jayabal, Ravikumar. (2024), "Optimization and Impact of Modified Operating Parameters of a Diesel Engine Emissions Characteristic Utilizing Waste Fat Biodiesel/Di-Tert-Butyl Peroxide Blend." Process Safety and Environmental Protection 186 694–705. https://doi.org/10.1016/j.psep.2024.04.019.

K, S. and K. Gottekere Narayanappa, (2020), Experimental analysis of a mini truck CRDI diesel engine fueled with n-Amyl alcohol/diesel blends with selective catalytic reduction (SCR) as a DeNOx technique under the influence of EGR. Energy Sources, Part A: Recovery, Utilization, and Environmental Effects, p. 1-16. https://doi.org/10.1080/15567036.2020.172844

Kannan, Rajesh, Sathiyamoorthi Ramalingam, Senthil Sampath, Mukilarasan Nedunchezhiyan, Damodharan Dillikannan, and Ravikumar Jayabal.(2024), "Optimization and Synthesis Process of Biodiesel Production from Coconut Oil Using Central Composite Rotatable Design of Response Surface Methodology." Proceedings of the Institution of Mechanical Engineers, Part E: Journal of Process Mechanical Engineering, February 8, https://doi.org/10.1177/09544089241230251.

Karthikeyan Subramanian, Sathiyagnanam Amudhavalli Paramasivam, Damodharan Dillikannan, Ravikumar Jayabal, (2023): "Effect of pilot fuel injection strategies and EGR on a CRDI diesel engine powered by simmondsia chinensis seed biodiesel-methyl acetate blend", Sustainable Energy Technologies and Assessments, Volume 58, 103345, https://doi.org/10.1016/j.seta.2023.103345.

Kim, H. Y., Ge, J. C., & Choi, N. J..(2019), Effects of Fuel Injection Pressure on Combustion and Emission Characteristics under Low Speed Conditions in a Diesel Engine Fueled with Palm Oil Biodiesel. Energies, 12(17), 3264. https://doi.org/10.3390/en12173264.

Kumar, P. and N. Kumar, Study of ignition delay period of n-Butanol blends with JOME and diesel under static loading conditions. Energy Sources, Part A: Recovery, Utilization, and Environmental Effects, 2018. 40(14): p. 1729-1736. 10.1080/15567036.2018.1486904

Lee, J.; Kwon, S.; Kim, H.; Keel, J.; Yoon, T.(2021) Machine Learning Applied to the NOx Prediction of Diesel Vehicle under Real Driving Cycle. Appl. Sci., 11, 3758. https://doi.org/10.3390/app11093758

Li, X., Liu, P., Wang, Z., Liu, P., Wei, X., Wu, Y.,... Lei, T. (2025). Catalytic cracking of biomass tar for hydrogen-rich gas production: Parameter optimization using response surface methodology combined with deterministic finite automaton. Renewable Energy, 241, 122368. https://doi.org/10.1016/j.renene.2025.122368

Liu, Jinlong & Huang, Qiao & Ulishney, Christopher & Dumitrescu, Cosmin E., (2021). "Machine learning assisted prediction of exhaust gas temperature of a heavy-duty natural gas spark ignition engine," Applied Energy, Elsevier, vol. 300(C).1. 10.1016/j.apenergy.2021.117413

Liu, H., Tang, L., Dou, Z., Wang, S., & Yu, D. (2025). Optimizing integrated hydrogen liquefaction with LNG cold energy: A thermoeconomic assessment, comparative analysis, and feasibility study with emphasis on composite curves and uncertainty scrutiny. Energy, 315, 134416. https://doi.org/10.1016/j.energy.2025.134416

Londhe, H., et al.,(2019), Testing of anisole and methyl acetate as additives to diesel and biodiesel fuels in a compression ignition engine. Fuel, 2019. 246: p. 79-92. https://doi.org/10.1016/j.fuel.2019.02.079

M. Vijay Kumar, A. Veeresh Babu, P. Ravi Kumar,(2018), The impacts on combustion, performance and emissions of biodiesel by using additives in direct injection diesel engine, Alexandria Engineering Journal, 57, Pp 509-516, https://doi.org/10.1016/j.aej.2016.12.016.

Mani, M., G. Nagarajan, and S. Sampath,(2010), An experimental investigation on a DI diesel engine using waste plastic oil with exhaust gas recirculation. Fuel, 89(8): p. 1826-1832. https://doi.org/10.1016/j.fuel.2009.11.009

Mohanrajhu, N., S. Sekar, Ravikumar Jayabal, and R. Sureshkumar.(2024), "Screening Nano Additives for Favorable NOx/Smoke Emissions Trade-off in a CRDI Diesel Engine Fueled by Industry Leather Waste Fat Biodiesel Blend." Process Safety and Environmental Protection 187 332–42. https://doi.org/10.1016/j.psep.2024.04.115.

Mohanrajhu, N., Sekar, S., Jayabal, R., & Sureshkumar, R. (2024). Impact of Aluminum Nitrate and Graphene Oxide Nanoplate on Performance and Emission Characteristics of a CRDI Diesel Engine Powered by Industrial Leather Waste Fat Biodiesel. International Journal of Automotive Technology. https://doi.org/10.1007/s12239-024-00205-5

Narayanan Subramanian, Ramesh Kasimani, (2022), Effects of antioxidant additive and injector hole number on combustion phenomenon of DI diesel engine operating with kapok methyl ester blends, Environmental Progress & Sustainable Energy, 41, https://doi.org/10.1002/ep.13825.

Prasada Rao, G. and L.S.V. Prasad, (2021), An attempt for improving the performance, combustion and exhaust emission attributes of an existing unmodified diesel engine powered with Palmyra biodiesel blends. International Journal of Ambient Energy, 43(1): p. 4424-4432. https://doi.org/10.1080/01430750.2021.190761

Qiu, Z., Chen, R., Gan, X., Wu, C., Yang, H.,... Zhao, Y. (2025). An Iterative Approach to Solve the Viscous Damper Temperature and the Torsional Vibration Amplitude of a Diesel Engine. Journal of Vibration Engineering & Technologies, 13(6), 437. doi: 10.1007/s42417-025-01983-7

Ramesh, A., et al.,(2019), Influence of hexanol as additive with Calophyllum Inophyllum biodiesel for CI engine applications. Fuel, 249: p. 472-485. 10.1016/j.fuel.2019.03.072

Ramesh, T; Sathiyagnanam, A P (2022) "Combined Effect of Compression Ratio and Fuel Injection Pressure on CI Engine Equipped with CRDi System Using Prosopis juliflora Methyl Ester/Diesel Blends" International Journal of Chemical Engineering, 2022, 4617664, https://doi.org/10.1155/2022/4617664.

Rangabashiam, D., et al.,(2020), Performance, emission, and combustion analysis on diesel engine fueled with blends of neem biodiesel/diesel/ additives. Energy Sources, Part A: Recovery, Utilization, and Environmental Effects, p. 1-11. 10.1080/15567036.2020.1764152

Sharbuddin Ali, S. and M.R. Swaminathan,(2020), Effective utilization of waste cooking oil in a diesel engine equipped with CRDi system using C8 oxygenates as additives for cleaner emission. Fuel, 275: p. 118003. https://doi.org/10.1016/j.fuel.2020.118003

Sharma, A., Y. Singh, and N.A. Kumar, Effect of fuel injection pressure and timing on Polanga (Calophyllum Inophyllum) biodiesel blends for engine performance and emissions analysis. Energy Sources, Part A: Recovery, Utilization, and Environmental Effects, 2019. 41(24): p. 3046-3057. https://doi.org/10.1080/15567036.2019.158369

Shin, D., Jo, S., Kim, H.J. et al. Application of Physical Model Test-Based Long Short-Term Memory Algorithm as a Virtual Sensor for Nitrogen Oxide Prediction in Diesel Engines. Int.J Automot. Technol. 24, 585–593 (2023). https://doi.org/10.1007/s12239-023-0049-y.

Shrivastava, P. and T.N. Verma,(2020) Effect of fuel injection pressure on the characteristics of CI engine fuelled with biodiesel from Roselle oil. Fuel, 265: p. 117005. https://doi.org/10.1016/j.fuel.2019.117005

Shubham Jain, Sukumar Purohit, Dipesh Kumar, Vaibhav V. Goud, (2021), Passion fruit seed extract as an antioxidant additive for biodiesel; shelf life and consumption kinetics, Fuel, 289, https://doi.org/10.1016/j.fuel.2020.119906.

Subramanian Karthikeyan, Paramasivam Sathiyagnanam Amudhavalli, Dillikannan Damodharan, (2024) Machine learning predictions on the output parameters of CRDI engines fueled with ternary blend: Chemical Industry & Chemical Engineering Quarterly, 31 (2). https://doi.org/10.2298/CICEQ240303025S.

Subramanian, K., et al., (2022), Prediction of thermal performance and exhaust emissions of a diesel engine fuelled with Simmondsia Chinensis oil methyl ester using ANN. International Journal of Ambient Energy, p. 1-14. https://doi.org/10.1080/01430750.2022.210318

Vellaiyan, S. (2025a). Optimization of hydrogen-enriched biodiesel-diesel dual-fuel combustion with EGR for sustainable engine performance. International Journal of Hydrogen Energy, 128, 85–94. https://doi.org/10.1016/j.ijhydene.2025.04.239

Vellaiyan, S. (2025b). Performance enhancement of a diesel engine using nanoparticle-enriched algae biodiesel-diesel blends with an electrostatic precipitator for nanoparticle emission control. Energy Conversion and Management, 326, 119457. https://doi.org/10.1016/j.enconman.2024.119457

Venu, H., L. Subramani, and V.D. Raju, (2019), Emission reduction in a DI diesel engine using exhaust gas recirculation (EGR) of palm biodiesel blended with TiO2 nano additives. Renewable Energy, 140: p. 245-263. https://doi.org/10.1016/j.renene.2019.03.078

Yang, R.; Xie, T.; Liu, Z.(2022), The Application of Machine Learning Methods to Predict the Power Output of Internal Combustion Engines. Energies, 15, 3242. https://doi.org/10.3390/en15093242

Zhou, L., Li, S., Jain, A., Sun, G., Chen, G., Guo, D.,... Zhao, Y. (2024). Optimization of Thermal Non-Uniformity Challenges in Liquid-Cooled Lithium-Ion Battery Packs Using NSGA-II. Journal of Electrochemical Energy Conversion and Storage, 22(4), 041002. https://doi.org/10.1115/1.4066725

Zhou, R.; Cao, J.; Zhang, G.; Yang, X.; Wang, X.(2023), Heat Load Forecasting of Marine Diesel Engine Based on Long Short-Term Memory Network. Appl. Sci., 13, 1099. https://doi.org/10.3390/app13021099

Zhou, X., et al.,(2020) Potential of n-butanol/diesel blends for CI engines under post injection strategy and different EGR rates conditions. Energy Conversion and Management, 204: p. 112329. https://doi.org/10.1016/j.enconman.2019.112329